Influence of salinity gradients on the diffusion of water and ionic species in dual porosity clay samples

Emmanuel Tertre, Thomas Dabat, Jingyi Wang, Sébastien Savoye, Fabien Hubert, Baptiste Dazas, Christophe Tournassat, Carl I Steefel, Eric Ferrage

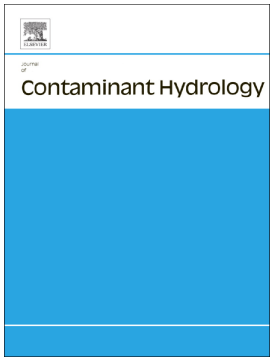

Influence of salinity gradients on the diffusion of water and ionic species in dual porosity clay samples

Emmanuel Tertre, Thomas Dabat, Jingyi Wang, Sébastien Savoye, Fabien Hubert, Baptiste Dazas, Christophe Tournassat, Carl I. Steefel, Eric Ferrage

PII: S0169-7722(24)00061-5

DOI: https://doi.org/10.1016/j.jconhyd.2024.104357

Reference: CONHYD 104357

To appear in: *Journal of Contaminant Hydrology*

Received date: 24 November 2023

Revised date: 19 March 2024

Accepted date: 24 April 2024

Please cite this article as: E. Tertre, T. Dabat, J. Wang, et al., Influence of salinity gradients on the diffusion of water and ionic species in dual porosity clay samples, *Journal of Contaminant Hydrology* (2023), https://doi.org/10.1016/j.jconhyd.2024.104357

Influence of salinity gradients on the diffusion of water and ionic species in dual porosity clay samples

Emmanuel Tertre[a,*], Thomas Dabat[a], Jingyi Wang[b], Sébastien Savoye[b], Fabien Hubert[a], Baptiste Dazas[a], Christophe Tournassat[c, d], Carl I. Steefel [d], Eric Ferrage[a].

[(a)] Université de Poitiers/CNRS, UMR 7285 IC2MP, Equipe HydrASA, 5 rue Albert Turpain, Bât. B8, TSA - 51106, 86073 Poitiers cedex 9, France.

[(b)] Université Paris-Saclay, CEA, Service d'Etude du Comportement des Radionucléides, 91191 Gif-sur Yvette, France

[(c)] Université d'Orléans/CNRS/BRGM, UMR 7327 ISTO, 45071 Orléans, France

[(d)] Lawrence Berkeley National Lab, Earth & Environmental Sciences Area, Berkeley, CA 94720 USA.

* Correspondance email: emmanuel.tertre@univ-poitiers.fr

Abstract

Most of the available data on diffusion in natural clayey rocks consider tracer diffusion in the absence of a salinity gradient despite the fact that such gradients are frequently found in natural and engineered subsurface environments. To assess the role of such gradients on the diffusion properties of clayey materials, through-diffusion experiments were carried out in the presence and absence of a salinity gradient using salt-diffusion and radioisotope tracer techniques. The experiments were carried out with vermiculite samples that contained equal proportions of interparticle and interlayer porosities so as to assess also the role played by the two types of porosities on the diffusion of water and ions. Data were interpreted using both a classical Fickian diffusion model and with a reactive transport code, CrunchClay that can handle multi-porosity diffusion processes in the presence of charged surfaces. By combining experimental and simulated data, we demonstrated that (i) the flux of water diffusing through vermiculite interlayer porosity was minor compared to that diffusing through the interparticle porosity, and (ii) a model considering at least three types of porous volumes (interlayer, diffuse layer interparticle, and bulk interparticle) was necessary to reproduce consistently the variations of neutral and charged species diffusion as a function of salinity gradient conditions.

Keywords: clayey porous media, water diffusion, ionic diffusion, salinity gradient, through-diffusion experiments, reactive transport modeling.

Introduction

Diffusion properties of water and aqueous solutes in clayey samples have been extensively studied, especially in the context of radioactive waste disposal in deep argillaceous rocks (Appelo and Wersin, 2007; Bourg and Tournassat, 2015; Charlet et al., 2017). Most of the data have been collected from laboratory experiments in which the electrolyte background was kept at constant concentration throughout the experiment, *i.e.* in the absence of a salinity gradient. Diffusion properties were probed by aqueous tracer species at very low concentrations compared to the electrolyte background concentration. Under these conditions, anionic and cationic tracers diffusion properties are considered to be independent of each other, and measured tracer diffusive fluxes can be interpreted using Fick's laws:

$$\frac{\partial C}{\partial t} = \frac{D_e}{\alpha} \cdot \frac{\partial^2 C}{\partial x^2} = \frac{D_e}{\varepsilon_{acc.} + \rho_{app.} R_d} \cdot \frac{\delta^2 C}{\partial x^2} \qquad \text{Equation 1}$$

where C is the aqueous concentration (mol m^{-3}), t is the time (s), α is the rock capacity factor, $\varepsilon_{acc.}$ is the diffusion-accessible porosity (dimensionless), $\rho_{app.}$ is the bulk dry density (kg m^{-3}), Rd is a distribution coefficient (m^3 kg^{-1}), which relates the tracer concentration adsorbed reversibly on the solid phase to its aqueous concentration, and D_e is the effective diffusion coefficient (m^2 s^{-1}):

$$D_e = D_P \varepsilon_{acc.} = D_0 \frac{1}{G} \varepsilon_{acc.} \qquad \text{Equation 2}$$

where D_P is the pore diffusion coefficient (m^2 s^{-1}), D_0 is the free-solution (aqueous) diffusion coefficient (m^2 s^{-1}), and G is the geometrical factor taking into account the tortuosity and constrictivity of the porous media, depending then on the geometrical organization of the porous medium (dimensionless).

Diffusion properties of clayey samples are markedly different for the anionic and cationic tracers. In particular, anionic and cationic tracers do not experience the same overall accessible porosity. Differences in accessible porosity can be related to the presence of the electrical double layer (EDL), *i.e.* a porosity domain next to the negatively charged surfaces of clay minerals such as smectite and illite in which electroneutrality is not achieved. EDL ion concentrations depend on the ionic strength of the bulk solution and distance from the surface considered. Anions are repelled from the region next to the surface where a negative electrostatic potential prevails. Conversely, cations are enriched in the diffuse layer. At an infinite distance from the charged surface, the solution is charge neutral and is commonly described as a bulk or free solution (or water). Because of their depletion in the EDL, diffusion rate of anions is decreased compared to aqueous neutral species that have access to the total porosity of the clayey sample, while diffusion rate of cations, which are enriched in the EDL, is increased. This interpretation of the difference in anionic and cationic tracer fluxes is further supported by the fact that an increase in ionic strength, which reduces anion exclusion at the vicinity

of charged surfaces, is responsible for an increase in anionic tracer diffusion. Conversely, cationic tracers diffusive fluxes also decrease because of the increased competition of electrolyte background cations with tracer cations for accumulation and charge compensation in the EDL (Tournassat and Steefel (2015, 2019), Charlet et al. (2017)).

Furthermore, in natural clayey formation, pore water composition is not always homogeneous throughout the formation. Differences in water composition in surrounding aquifers can then create salinity gradients in clay formations (Gonçalvès et al., 2004; Gaucher et al., 2006; Gueutin et al., 2007; Mazurek et al., 2011; Pearson et al., 2011; Wersin et al., 2016), and these gradients may represent steady-state conditions, or not. In the lifetime of an underground repository facility, interactions of waste and barrier materials are foreseen to create salinity gradients through a variety of mechanisms in surrounding clay materials. Under these conditions, a coupling of anionic and cationic tracer diffusion with the diffusion of electrolyte background species is inevitable (Appelo et al., 2010; Tournassat and Steefel, 2019 and 2020).

Diffusion data obtained under salinity gradients are less common in literature than those obtained at constant electrolyte background concentration. Some authors are however obtained data for bentonites and geosynthetic clay liners under salinity gradients, especially by using salt-diffusion techniques in the context of conventional waste containment applications and/or salt transfer in soils (Kemper and Schaik, 1966; Lake and Row, 2000; Malusis and Shackelford, 2002; Bohnhoff and Shackelford, 2014 among others). In these cases, the authors investigated then the diffusion of the major species responsible for the background electrolyte concentration gradient. In these experiments, aqueous species diffusive fluxes are governed by that of the slowest ion present in the system, usually the anion because of the anion exclusion effect. In binary systems, i.e. in the presence of only one type of anion and cation in the system, including the type of cation present on the clay mineral surfaces, cation diffusion is equal to that of the anion. This observation, which differs from what is observed for anionic and cationic tracers in the absence of background electrolyte concentration gradient, agrees with the electroneutrality condition in aqueous solutions. Mobility of the dissolved salt increases also with the increase of the salinity gradient, which is in agreement with a reduced anionic exclusion as the ionic strength increases. Note that influence of a background electrolyte concentration gradient on the diffusion of anionic and cationic species at trace concentrations has also been rarely investigated. Notable exceptions are the DR-A in situ diffusion experiment conducted at the Mont-Terri laboratory (Soler et al., 2019), and an “uphill” diffusion experiment of a $^{22}Na^{+}$ tracer in a compacted sodium montmorillonite (Glaus et al. 2013). These two studies demonstrated the marked influence of background electrolyte concentration

gradient on tracer diffusion, and thus the necessity to understand the couplings between diffusion of several charged species present at contrasting concentrations and experiencing different concentration gradients. The experiment from Glaus et al. (2013) also demonstrated the importance of considering diffusion processes occurring in the porosity next to the charged surface of clay minerals (i.e., the porosity associated to the EDL of particles).

Depending on dry density (i.e. compaction), salinity, and the nature of the clay minerals, EDL porosity properties vary considerably primarily because of differences in the pore size distribution and electrostatic potential. Montmorillonite, which is the most studied clay mineral in the diffusion literature, as in Glaus et al. (2013), is a low-charge clay mineral that exhibits swelling properties, meaning that the number of water molecules in-between montmorillonite layers varies as a function of the water potential. Depending on salinity, applied pressure, temperature, and hydration, the number of water molecules varies from the equivalent of one (~3 Å), two (~6 Å), or three (~9 Å) monolayers (crystalline swelling regime with the presence of interlayer porosity, which can be seen as an extremely contracted EDL porosity), or to layer-to-layer separation distance above 30 Å (osmotic swelling regime with the presence of a true EDL porosity). The abrupt transition from the osmotic swelling regime to that of the crystalline swelling regime eventually results in a complete rearrangement of the pore size distribution (Abend and Lagaly, 2000; Tournassat and Appelo, 2011; Liu, 2013; Massat et al., 2016). Such dynamic processes make it difficult to determine accurately the different porous volumes (interlayer, diffuse layer interparticle, and bulk interparticle) present in compact montmorillonite samples. Consequently, it is difficult to attribute diffusion transport properties to each of these porosity types unequivocally, particularly when a salinity gradient is present that creates differences in microstructure along the gradient. However, in contrast to montmorillonite, vermiculite, which is a high-charge smectite, exhibits only crystalline swelling, even for samples made with very fine particles (e.g., < 0.2 µm particles; (Faurel, 2012)). Then, using such particles to prepare clayey porous media with the objective to control the distribution of interlayer and interparticle porosity volumes is ideal.

In this current study, through-diffusion experiments were carried out with nearly isotropic porous media consisting of Na-vermiculite particles. The originality of the study was to perform these experiments in the presence and absence of salinity gradients, to assess their influence on diffusion properties of the porous media. Thanks to the use of vermiculite particles, additional objective of this study is to precise the roles played by interlayer and interparticle porosities on the diffusion of water and ions as a function of background electrolyte gradients. Data were interpreted using a semi-analytical solution of Fick's laws, and also with a reactive transport code, CrunchClay, which can

handle multi-porosity diffusion processes in the presence of charged surfaces and EDL (Tournassat and Steefel, 2019; Steefel and Tournassat, 2021).

Material and methods

Material. Porous media consisting of saturated Na-vermiculite particles having a 0.1-0.2 µm size fraction were prepared for use in the experiments. All details concerning the origin of the raw material, the preparation method to obtain the appropriate size fraction from centimeter natural monocrystals, crystal chemistry, and morphological parameters have been detailed in Reinholdt et al. (2013). The 0.1-0.2 µm size fraction presents an aspect ratio (thickness over average diameter) close to 0.1, a total cationic exchange capacity of 220 meq/100 g, from which 60 meq/100 g can be attributed to external (as opposed to interlayer) surfaces (Dzene et al., 2016), and a total external specific surface area of 100 $m^2 g^{-1}$ (Reinholdt et al., 2013).

Compacted samples having a total porosity of 0.5 were prepared from the 0.1-0.2 µm size fraction dried at 60 °C and sieved through a 50 µm mesh to remove the coarsest aggregates. These samples were prepared by uniaxial compaction using a hydraulic press in polyetherketone (PEEK) tubes (diameter = 0.95 cm, height = 7 cm) (Tertre et al., 2018). This preparation procedure allowed for an isotropic organization of the particles (Dabat (2019), Asaad et al. (2021)). The particle size fraction and sample dry density chosen resulted in the interlayer and interparticle porosities being equal to 0.25 (Asaad et al., 2021).

Through-diffusion experiments. The details of the set-up of through-diffusion experiments have been described in previous works to study the mobility of water (HDO or HTO tracers) and ions (Na^+ and Cl^-) in clayey samples in the absence of background electrolyte concentration gradient (Van Loon et al., 2003; Savoye et al., 2012; Tertre et al., 2018; Wang et al., 2022). Experiments were carried out with 50 mL reservoirs connected to the clay sample. They were conducted at 20 ± 2 °C in the presence and absence of NaCl concentration gradients. Two experiments were conducted with a constant salinity at 1 M and 10^{-2} M, for which the diffusion of HTO, $^{36}Cl^-$ and $^{22}Na^+$ radioisotopes was monitored. Two other experiments were conducted with salinity gradients imposed by 1 M and 10^{-2} M NaCl in the upstream reservoirs and deionized water (< 10^{-5} M NaCl) in the downstream reservoirs (Table 1). In these experiments, the diffusion of HDO, Na^+, and Cl^- was monitored. For experiments carried out in the absence of a salinity gradient, upstream reservoirs were not replaced during the experiments while downstream reservoirs were replaced when tracer mass activities reached 1 % of

the concentration present in the upstream reservoir. This procedure is commonly used in through-diffusion experiments to avoid an increase in tracer activities in downstream reservoirs that would influence the overall diffusion gradient through the sample with time (Glaus et al., 2007). In experiments that included a NaCl concentration gradient, upstream and downstream reservoirs were replaced at each sampling step. In the presence of salinity gradients, determination of the constant reservoir weights showed negligible osmotic water flux during the experiments.

Aqueous concentration measurements. HDO concentrations were determined by water isotope analysis (LWIA DLT-100, Los Gatos Research®), and the amount of HDO diffusing in the downstream reservoir was calculated by accounting for the HDO concentration that was naturally present in ultrapure water, *i.e.* 1.65 10^{-2} M (Tertre et al., 2018). Uncertainty in the HDO concentration was estimated at 10 % (2σ standard deviations) based on the variation of 5 replicate measurements on the same sample. Aqueous Na^+ concentrations were measured using an atomic absorption spectrophotometer (Varian® AA240FS). Samples were prepared in 2 % HNO_3 solution and 2 g L^{-1} potassium chloride solution to account for possible interference during acquisition. Cl^- aqueous concentrations were measured by liquid ionic chromatography (ICS 1000, Dionex®) by using an AS9-HC column (Thermo Scientific®) and a 5 10^{-3} M Na_2CO_3 eluant solution. An uncertainty (2σ) of 10 % was found for Na^+ and Cl^- concentrations, based on 5 replicate measurements on a selection of analyzed solutions.

HTO and $^{36}Cl^-$ activities were measured by β^- liquid scintillation (Packard Tricarb® 2700) and $^{22}Na^+$ activities were obtained using γ counting (Packard® 1480, Wizard). Both technics led to detection limits of around 0.1 Bq, and total uncertainties (2σ) of 10 %.

Data analysis and modeling. Effective diffusion coefficient (D_e) and rock capacity values (α) of clay porous media were obtained by least-square fitting of the experimental results of the diffusive flux incoming in the downstream reservoir using a semi-analytical solution of the diffusion Equation 1 (Descostes et al., 2008; Tertre et al., 2018). In this case, the following boundary and initial conditions where the concentration in the upstream reservoir is left free to decrease are considered:

$C(x,t) = 0$, $t = 0$

$C(x,t) = C_0$ $x = 0$, $t = 0$

$C(x,t) = 0$ $x = L + 2l$, $t > 0$

where L and l are, respectively, the sample and stainless-steel filters thicknesses (m). The MIEDE code (Radwan et al., 2006) was used, which solves the diffusion equations analytically in Laplace space and then inverts them numerically for the purposes of parameter estimation by means of the

De Hoog algorithm (Moridis, 1998). The semi-analytical solution was given in Didierjean et al. (2004). This mathematical resolution makes it possible to obtain diffusion parameters of the clay porous media while taking into account (i) the geometric and diffusion properties of stainless-steel filters used in the experiments and (ii) the possible decrease of the tracer concentration in the upstream reservoir due to its consumption by diffusion in the porous media. For these calculations, filters characteristics were the following: thickness = 1.66 mm, diameter = 9.5 mm, porosity = 0.28, and $\frac{1}{G}$ = 0.38 as reported by Glaus et al. (2008) for a water tracer. Uncertainties associated with clay diffusion parameters were obtained by considering uncertainties associated with the concentration (or activity) measurements (see Table 1).

Reactive transport modelling was conducted to unravel the respective contributions of interlayer *vs.* interparticle porosities (dual porosity) on the measured diffusion properties, as well as to estimate the influence of coupling terms related to electrostatic interactions at charged clay mineral surfaces. Fig. 1 illustrates the concept of the dual porosity used in our approach to describe/predict data obtained with vermiculite samples. Simulations were carried out using CrunchClay (Tournassat and Steefel, 2015, 2019, 2020; Steefel and Tournassat, 2021), which takes into account the EDL properties to evaluate overall diffusive fluxes using the Nernst-Planck equation instead of the Fick's equation. In the absence of advection and electrical current injection, the Nernst-Planck diffusive flux equation simplifies into:

$$J_i = -\frac{\varepsilon}{G_i} D_{0,i} c_{i,0} A_i \frac{\partial \ln(\gamma_i c_{i,0})}{\partial x} + \frac{\varepsilon}{G_i} D_{0,i} z_i c_{i,0} A_i \frac{\sum_j \frac{1}{G_j} D_{0,j} z_j c_{j,0} A_j \frac{\partial \ln(\gamma_j c_{j,0})}{\partial x}}{\sum_k \frac{1}{G_k} D_{0,k} z_k^2 c_{k,0} A_k} \qquad \text{Equation 3}$$

where the subscripts i, j and k refer to the individual aqueous species, for which specific activity coefficients (γ), charge (z), geometrical factor (G) and accumulation factor (A) values are considered. The accumulation factor represents the ratio of the average concentration in the considered pore compared to that of the bulk water, which is not influenced by the presence of a diffuse layer. Because vermiculite surfaces are negatively charged, the porosity fraction next to the vermiculite surfaces are enriched in cations (A > 1) and depleted in anions (A < 1) compared to a bulk porosity fraction. The accumulation factor values are evaluated using a mean electrostatic model, which is a simplification of the Poisson-Boltzmann model. The full details on the model can be found in Tournassat and Steefel (2019). Calculations with increasing level of complexity were carried out to characterize the influence of diffusion paths in interparticle (bulk and EDL) and interlayer porosities. Geometric details of these calculations are given in S.I.1 and Fig. S.I.1. All calculations were carried out with self-diffusion coefficient values (D_0) at 20 °C equal to 2.1 10^{-9}, 1.7 $10^{-9,}$ and 1.3 10^{-10} m^2 s^{-1} for HDO/HTO, Cl^- and Na^+, respectively (Mills and Lobo, 1989). Note that these CrunchClay calculations

were carried out as predictive simulations to identify the primary diffusion mechanisms, that is, not with the intent of fitting the experimental data.

Results and discussion

All flux data reported in the following section were normalized to the concentration of the relevant species in the upstream reservoir and the sample surface area perpendicular to the diffusion direction (*i.e.*, flux in m day^{-1}) so that results obtained with different conditions could be compared more easily. Data obtained for HTO/HDO and ions (*i.e.*, anions and cations) are reported in Figs. S.I.2 and S.I.3, respectively.

HTO and HDO diffusion. Instantaneous fluxes and cumulative total amounts for HDO/HTO measured in the downstream reservoirs were compared with those fitted by MIEDE (Fig. S.I.2) for the four salinity conditions (with and without salinity gradients). HTO and HDO tracers exhibited the same diffusion properties (Table 1) for all investigated systems given the uncertainties estimated for diffusion coefficients, thus demonstrating a negligible influence of background NaCl electrolyte concentration on water molecule diffusion properties. HDO and HTO rock capacity factors were equal to the total porosity of the sample, which was in agreement with literature results on HTO and HDO diffusion in swelling and non-swelling clay materials (Bourg and Tournassat, 2015). This result was also in agreement with the connectivity of all interlayer or interparticle pores present in the samples. In the limit of the experimental error bands, effective diffusion coefficient values are independent of the ionic strength and the presence or absence of a salinity gradient. The absence of change in the D_e value with a change in salinity is in agreement with some of the literature data (Glaus et al., 2007; González Sánchez et al., 2008; Melkior et al., 2009; Glaus et al., 2010; Bestel et al., 2018). This would suggest that the influence on D_e of fluid viscosity decrease with salinity increase (Wigger and Van Loon, 1998) was negligible in our experimental conditions (< 1 M NaCl). However, this result contrasts with other data reported in the literature (Van Schaik and Kemper, 1966; Kemper and Van Schaik, 1966; Muurinen et al., 1989; Lake and Rowe, 2000; Malusis and Shackelford, 2002; Heister et al., 2005) where changes in D_e values with changes in salinity were observed. These latest studies were carried out with bentonite, *i.e.* with smectitic (mostly montmorillonite) clayey materials exhibiting osmotic swelling properties. Smectitic materials are prone to exfoliation of individual layers, which may be responsible for the presence of small pore throats with widths below a few Debye lengths (i.e., typically < 30 Å considering a fluid salinity at 10^{-2} M) that result in semi-permeable membrane properties. In turn, this behavior can modify the organization of the smectitic porous media when subjected to variations in salinity, thus leading to changes in diffusion properties

contrasting with the behavior observed for vermiculite for which the absence of osmotic swelling prevents such re-organization. Self-diffusion of water in vermiculite interlayers is slower than in montmorillonite interlayers (Assad et al., 2021), but D_e values obtained for Na-vermiculite samples (Table 1) were systematically higher by a factor ~5 compared to D_e values obtained with Na-montmorillonite or Na-bentonite samples having the same total porosity values (Garcia Gutierrez et al., 2004; Melkior et al., 2009; Glaus et al., 2010). The flux of water tracers diffusing through charged clayey porous media is markedly influenced by sample microstructure, including pore and pore throat size distribution. Then, in the vermiculite samples used in this present study, the diffusive flux is mainly governed by the interparticle volume, with the interlayer flux playing only a marginal role, as previously reported by Tertre et al. (2018) and Asaad et al. (2021).

$^{36}Cl^-$ and Cl^- diffusion. In the absence of a salinity gradient, $\alpha(^{36}Cl^-)$ values ranged from 0.25 to 0.4, and were lower than the total porosity (0.5) of the samples for the two tested salinity conditions (Table 1, Fig. S.I. 3a). These results are in agreement with a partial exclusion of anions from part of the porosity, as commonly reported in the literature (Glaus et al., 2010; Tournassat and Appelo, 2011; Bourg and Tournassat, 2025). Anions are expected to have little to no access to the interlayer space of swelling clays in a 2 WL hydrated state (Birgersson and Karnland, 2009; Hedström and Karnland, 2012; Rotenberg et al., 2014; Tournassat et al., 2016). Accordingly, the maximum accessible porosity for anions in our sample should be about 0.25, corresponding to the interparticle porosity. The upper range of α values may indicate the presence of slight adsorption of anions on the external surfaces of vermiculite particles or a limited but significant access of $^{36}Cl^-$ to interlayer spaces. $D_e(^{36}Cl^-)$ decreased by one order of magnitude while salinity decreased by two orders of magnitude (Table 1 and Fig. 2). This variation was consistent with an increased repulsion of $^{36}Cl^-$ from interlayer and/or EDL with a decrease in ionic strength as commonly reported in the literature for anions diffusion in illitic and smectitic materials (Van Loon et al., 2007; Glaus et al., 2010; Chen et al., 2018).

In the presence of a salinity gradient (aqueous upstream reservoirs of 10^{-2} or 1 M NaCl), α and D_e values obtained for Cl^- were not significantly different from those obtained without such gradient in the limit of experimental uncertainties (see Table 1 and Fig. 2). As for conditions with no salinity gradient, slight adsorption of Cl^- cannot be ruled out completely when a salinity gradient is imposed. Anyway, the main result brought by these data is that the anion (*i.e.*, Cl^- in our case) controls the diffusion of the NaCl salt in such salinity gradient conditions.

$^{22}Na^+$ and Na^+ diffusion. In the absence of salinity gradients, the $^{22}Na^+$ α value was significantly higher than the total porosity of the sample in the experiment conducted at 1 M NaCl (3.2 *vs.* 0.5 respectively; see Table 1), which is in agreement with $^{22}Na^+$ adsorption through ion-exchange reactions as commonly reported in the literature for other charged clayey materials (Glaus et al., 2010). In the presence of 10^{-2} M NaCl, constant $^{22}Na^+$ activity in the upstream reservoir could not be maintained (Fig. S.I.4 a) and steady-state conditions (*i.e.*, constant flux) in the downstream reservoir were never achieved (Fig. S.I.4 b). Moreover, $^{22}Na^+$ mobility in the clay medium was limited by its mobility in the stainless filters and then only the lower limit of the diffusion parameter values could be estimated using MIEDE (α>750; D_e>2 10^{-9} $m^2.s^{-1}$). The high α value corresponds to high $^{22}Na^+$ adsorption in these conditions. This behavior can be explained by the large proportion of the interlayer porosity (~ 0.25) as compared to the total porosity (~ 0.5) in the sample, and thus the high concentration of $^{22}Na^+$ that could be adsorbed in the interlayer porosity. Such an effect has been already reported for the diffusion of $^{22}Na^+$ in montmorillonite-rich samples but at a lower level than in this case (Glaus et al., 2010). The enhancement of this effect in the case of vermiculite could be due to the absence of osmotic swelling and/or its higher structural charge compared to that of montmorillonite. The increase of the $D_e(^{22}Na^+)$ value with decreasing ionic strength is in agreement with literature data obtained with montmorillonite and bentonite samples (see Fig. 2).

In the presence of a salinity gradient with 1 M NaCl in the upstream reservoir, Na^+ diffusion parameters were very similar to those obtained in the absence of salinity gradient ($D_e(Na^+)$ = 2.1 10^{-10} m^2 s^{-1} *vs* 2.3 10^{-10} m^2 s^{-1} respectively). In contrast, values differed drastically in the experiment carried out with a 10^{-2} M upstream reservoir with and without salinity gradients (Table 1). $D_e(Na^+)$ values were at least two orders of magnitude lower in the presence of a salinity gradient than without (3.5 10^{-11} m^2 s^{-1} *vs* D_e > 2 10^{-9} m^2 s^{-1} respectively). Using a 1 M NaCl concentration for the upstream reservoir (with the downstream reservoir being deionized water), diffusion parameters obtained for Na^+ are very close to those obtained for Cl^-, confirming that the diffusion of the NaCl salt under salinity gradient is controlled primarily by diffusion of the anion (e.g., Cl^-) as previously suggested by the analysis of Cl^- diffusion parameters. Furthermore, $D_e(Na^+)$ value is about 2 times higher than that of $D_e(Cl^-)$ for experiments conducted with a salinity gradient using a low salinity for the upstream reservoir (*i.e.*, 10^{-2} M). Because of the electroneutrality requirement, this result suggests that ionic species other than Na^+ and Cl^- accounted for some of the charge compensation via diffusion during this specific experiment, and that a more complicated coupled process occurred. Some authors mentioned also that other aqueous species than those impose experimentally (i.e., NaCl in the upstream reservoir in our case) can assure the electroneutrality of aqueous reservoirs when through-diffusion experiments of salt were performed at low ionic strength (i.e., < 0.1 M). For example,

during a diffusion experiment of 8 10^{-2} M NaCl solution through geosynthetic clay liners, Lake and Rowe (2000) mentioned that SO_4^{2-} species, naturally present initially in the porosity of the clay liners, diffuse towards aqueous reservoir explaining a mobility difference of around 50% between Na^+ and Cl^-. Furthermore, Malusis and Schackelford (2002) measured also a difference of mobility between K^+ and Cl^- during diffusion of a 4.10^{-3} M KCl solution through a semipermeable clay membrane up to 60%, due to Na^+ species remaining initially in the porosity of the clay membrane. As far as the experiment performed here with a salinity of 10^{-2} M is concerned, pH variation measured between upstream and downstream reservoirs (i.e., around 1 unit pH) during experiments, impacting then possible equilibrium with carbonates (experiments were not performed under inert atmosphere), could be at the origin of the charge imbalance considering only Na^+ and Cl^- species. However, the quantification of such effect is far from trivial due to the very low difference of aqueous carbonates concentration between the two aqueous reservoirs and other experiments could be planned in the future to confirm this assumption. Furthermore, such a difference between Cl^- and Na^+ fluxes is not observed in the experiment with an upstream reservoir at 1 M NaCl, because of the higher concentration and fluxes values, which limited the influence of presence of other ionic species as mentioned above for low ionic strength conditions. Finally, with the presence of salinity gradients, the evolution of $D_e(Na^+)$ with the salinity of the upstream reservoir is reversed compared to the case without such gradient (see Fig. 2). This observation is in agreement with data reported by Lake and Rowe (2000) for the diffusion of NaCl through bentonite samples in the presence of a salinity gradients (Fig. 2). It is enhanced here probably because of the larger range of salinity conditions tested, from 10^{-2} to 1 M in this study *vs* from 8 10^{-2} to 2 M in Lake and Row (2000), and the use of vermiculite samples enhancing cation adsorption in the interlayer volume.

Reactive transport modeling. For illustration, Fig. 1 shows the concept of the dual-porosity used in this study to interpret the data. First, we considered that interparticle porosity ($\varepsilon_{interparticle}$) was responsible for the HTO/HDO flux measured in all experiments (Assad et al., 2021). Interlayer porosity ($\varepsilon_{interlayer}$) was considered to have a diffusivity of zero, or equivalently a very high geometrical factor ($i.e., G$) value. To compensate for this absence of diffusive flux in interlayers, the geometrical factor in the bulk porosity ($G_{interparticle}$) of the sample was set to:

$$\frac{1}{G_{interparticle}} = \frac{1}{G_{miede}} \times {\varepsilon_{tot}}/{\varepsilon_{interparticle}} = 2\frac{1}{G_{miede}} \qquad \text{Equation 4}$$

in which G_{MIEDE} is the geometrical factor value fitting HDO/HTO experimental data with MIEDE code (see Table 1), ε_{tot} is the total porosity of the sample (i.e., fixed to 0.5 in our case), and $\varepsilon_{interparticle}$ is fixed to 0.25 in our case.

A perfect agreement was obtained between the flux fitted by MIEDE and the flux predicted by CrunchClay ('CrunchClay 2 porosities' model) for the experiments performed without NaCl concentration gradients using these assumptions (see Fig. 3 for HTO at 10^{-2} M NaCl and 1 M NaCl). Overall the rock capacity factor (*i.e.*, α) was the same in the two types of simulation:

$$\alpha = \varepsilon_{tot} = \varepsilon_{interparticle} + \varepsilon_{interlayer} \quad \text{Equation 5}$$

and the enhanced diffusivity of the interparticle porosity compensated for the absence of diffusivity in the interlayer according to the:

$$D_e = \varepsilon_{interparticle} \frac{1}{G_{interparticle}} D_O = \varepsilon_{tot} \frac{1}{G_{MIEDE}} D_O \quad \text{Equation 6}$$

In the presence of a NaCl concentration gradient between 1 M in the upstream reservoir and 0.005 M in the clay and downstream reservoir (attempts to decrease further the latest concentration resulted in calculation convergence issues), an increase of HDO diffusive flux (maximum 10%) was predicted using this model (see Fig. 4A). This increase was related to the presence of an activity gradient which is implicitly taken into account in CrunchClay and which participates to an enhancement of diffusion according to the full treatment of the Nernst-Planck equation (Tournassat and Steefel, 2019, 2020). Indeed, additional CrunchClay simulation with the cancellation of the influence of activity coefficient gradients predicts a reduction of the flux of about 3 % compared to that predicted by the initial model taking into account activity gradients (see S.I.5 for illustration in the case of the presence of a NaCl concentration gradient between 1 M in the upstream reservoir and 0.005 M in the clay and downstream reservoir). The slight increase of diffusivity predicted by the model taking into account activity gradients was not observed in the experiments, but measurement uncertainties can be invoked to explain this absence of observation. Another explanation is related to viscosity increase with NaCl concentration, which CrunchClay does not take into account. This correction would be necessary to compute correct D_0 values. If this effect was considered, the D_0 value should be corrected by a factor of approximately 0.9 at NaCl 1 M compared to pure water (Appelo et al., 2010). This factor is commensurable with, but opposite to, the predicted increase in diffusivity in the presence of a concentration gradient, and these two effects might indeed cancel each other.

Na^+ and Cl^- diffusive fluxes in the presence of a NaCl concentration gradient were first predicted with the same model as for HTO ('CrunchClay 2 porosities' model) without changing any parameter (Fig.

4). For the experiment with 1 M NaCl in the upstream reservoir, steady state flux predictions were in reasonable agreement with measurements although showing a slight underestimation (~25 % ; see Fig. 3A). The mean electrostatic model implemented in CrunchClay for the calculation of aqueous concentration in the EDL porosity influenced by surface charges does not make it possible to exclude a species completely for that porosity. Consequently, Cl^- interlayer concentration amounted to 8 10^{-10} M at 10^{-4} M interparticle bulk Cl^- concentration, and 0.06 M at 0.88 M interparticle bulk Cl^- concentration, which were respectively the minimum and maximum concentration reached in the simulation.. While Cl^- access to the interlayer is questionable (Rotenberg et al., 2014; Tournassat et al., 2016), this modeling issue does not influence the fluxes calculated at the transitory state (i.e., no retardation was predicted) and at steady state that are representative of interparticle diffusivity only, because diffusivity was set to zero for all species in the interlayer. Furthermore, the slight difference observed in the predictions at 1 M and 10^{-2} M NaCl gradient conditions corresponds to the influence of the activity term in the Nernst-Planck diffusion equation: Na^+ and Cl^- activity coefficients are lower at high ionic strength than at low ionic strength, and thus overall diffusion occurs at counter-gradient of activity coefficients. Consequently, predicted Na^+ and Cl^- diffusive fluxes are slightly reduced at higher ionic strength using the 'CrunchClay 2 porosities' model (*e.g.*, 1.0 10^{-3} *vs* 1.05 10^{-3} m/day for Cl^- flux using 1 and 10^{-2} M upstream reservoirs respectively; see the comparison in Figs. 3A and 3B). Note, however, that the extent of this ionic strength effect is negligible compared to measurement uncertainties.

Using CrunchClay models, Na^+ and Cl^- had the same predicted steady-state fluxes because of the electroneutrality requirement. The fluxes normalized to the concentration in the upstream reservoir were almost the same for experiments with 1 M and 0.01 M NaCl concentration gradients from the upstream to the downstream reservoir, save for the above-mentioned minor influence of activity coefficient gradient (Figs. 3A and B). Note that this prediction was not at all in agreement with experimental results, for which Na^+ and Cl^- steady-state fluxes normalized to the upstream concentration were about 3 to 5 times lower with an upstream concentration of 10^{-2} M than with an upstream concentration of 1 M. This comparison demonstrated the need to consider an additional process in the interparticle porosity that hinders the diffusion of Na^+ and Cl^- at low ionic strength.

The average distance between vermiculite particles ($\delta_{interparticle}$) can be approximated with the following equation:

$$\delta_{interparticle} = \frac{V_{interparticle}}{A_{external}/2} = \frac{2\,\varepsilon_{interparticle}\,V_{sample}}{V_{vermiculite}\,\rho_{vermiculite}\,SSA_{external}} \qquad \text{Equation 7}$$

where V_{sample} is the sample volume (in m^3), $V_{interparticle}$ is the interparticle volume in the sample (in m^3), $V_{vermiculite}$ is the volume of vermiculite including interlayer volume in the sample (in m^3),

$A_{external}$ is the external surface of vermiculite particles (in m^2), $\rho_{vermiculite}$ is the vermiculite density that includes interlayer volume (in kg m^{-3}), and $SSA_{external}$ is the specific external surface area (in m^2 kg^{-1}). Equation 7 yields a $\delta_{interparticle}$ value about 3.7 nm, which is commensurate with 4 Debye lengths in a 0.1 M NaCl background electrolyte. Therefore, for concentrations below 0.1 M, interparticle pores were mostly occupied by the diffuse layers extending from the surfaces bordering the pores (Tournassat and Appelo, 2011). Under those conditions, varying the size of the diffuse layer as a function of ionic strength was not practicable within CrunchClay because, as ionic strength decreased below 0.1 M, the extent of the diffuse layer porosity calculated as twice the Debye lengths exceeded the total porosity. There is no simple and accurate solution to this problem, which has been discussed in detail in Tournassat and Steefel (2019). In the following, we considered as an approximation that the diffuse layer occupied approximately 90 % of the interparticle porosity. The corresponding simulation considered thus three different types of porosity domain: interlayer, bulk interparticle, and diffuse layer interparticle (*i.e.*, 'CrunchClay 3 porosities' model). As expected, the predicted HDO/HTO diffusive fluxes were not influenced by this porosity redistribution (Fig. 4). In contrast, Na^+ and Cl^- diffusive fluxes were reduced because of the resistance to diffusion at the low concentration boundary of the sample due to the negative electrostatic potential of the diffuse layer porosity for which Cl^- accessibility was hindered. Then, because of the electroneutrality requirement, Na^+ diffusion was hindered as well. The effect was more pronounced for the 0.01 M gradient (Fig. 4B) than for the 1 M gradient (Fig. 4A) in agreement with the increase of anion repulsion from the EDL with decreasing ionic strength.

Finally, without parameter modification, our 'CrunchClay 3 porosities' model predicted relatively well the relative behavior of $^{22}Na^+$ and $^{36}Cl^-$ diffusion at constant background NaCl concentration (Fig. 3). First, the $^{36}Cl^-$ steady-state flux was much lower than that of $^{22}Na^+$ (Fig. 3A) because of anion exclusion from the diffuse layer of the interparticle porosity and of cation diffuse layer enhanced diffusion at charge surface of interparticle pores (Glaus et al., 2010; Tournassat and Steefel, 2015). Second, $^{36}Cl^-$ diffusion was more reduced at low ionic strength than it was at high ionic strength (compare Fig. 3A with Fig. 3B), which can be explained by its lower concentration in the diffuse layer at low ionic strength (see *e.g.* Tournassat and Appelo, 2011). Third, as expected from qualitative analysis of experimental data, $^{22}Na^+$ diffusion flux at 10^{-2} M constant background NaCl concentration did not reach a steady state in the time frame of the simulation (Fig. 3B) because of $^{22}Na^+$ enrichment in the diffuse layer and the interlayer of vermiculite. Fourth, at 1 M constant background NaCl condition, the predicted $^{22}Na^+$ steady flux was ~20 % higher than the measured one (Fig. 3A). This discrepancy can be resolved with the consideration of different D_0 values for Na^+ in the bulk and EDL porosities: a reduction of ~30 % of $D_0(^{22}Na^+)$ in the EDL compared to bulk porosity allows us to

perfectly reproduce experimental data (see Fig. 3A). Such differences in self-diffusion coefficient are in agreement with molecular dynamic simulations results (Le Crom et al., 2022). The predicted time that was necessary for the fluxes to reach steady-state was otherwise in good agreement with experimental data, particularly considering that the simulation was a blind prediction from a model that did not match perfectly our NaCl diffusion data.

Final remarks. The modeling of the experiments showed that even though interlayer porosity is accessible to water tracer (HDO and HTO), the flux of water diffusing through this volume is not significant compared to that diffusing in the interparticle porosity of our dual-porosity vermiculite samples, which had equal proportions of interparticle and interlayer porosities and a high layer charge.

The mobility of Cl^- depends strongly on the salinity of the pore water in experiments carried out at constant salinity conditions (tracer experiments with $^{36}Cl^-$) and in the presence of a NaCl concentration gradient. In the latter case, the diffusion flux of Na^+ was governed by that of Cl^- because of the electroneutrality requirement, thus leading to a negligible flux of cation in the interlayer porosity. The consideration of three types of porous volumes (interlayer, diffuse layer interparticle, and bulk interparticle) and the influence of surface charge on diffusion properties was necessary to predict the observed differences of diffusion properties as a function of experimental conditions. These differences include a difference in diffusive flux by a factor of 50 for Na^+ salt diffusion coefficient, obtained using a salinity gradient using 10^{-2} mol L^{-1} for the upstream reservoir (and deionized water for the downstream reservoir), as compared to $^{22}Na^+$ tracer diffusion coefficient obtained using a constant NaCl concentration equal to 10^{-2} mol L^{-1} in the clay porous media.

Supporting information (S.I.)

S.I.1 details CrunchClay calculations and Fig. S.I.1 is a schematic representation of the spatial discretization of the diffusion system used to perform reactive transport modeling using CrunchClay.

S.I.2 reports HDO and HTO through diffusion experimental data and MIEDE analysis. These data compare the instantaneous fluxes and the cumulative total amounts of HDO/HTO measured in the downstream reservoirs with those fitted by MIEDE (see text for details). Data are reported for the four salinity conditions (with and without salinity gradients).

S.I.3 reports anionic ($^{36}Cl^-$ and Cl^-) and cationic tracers ($^{22}Na^+$ and Na^+) data from through-diffusion experiments and MIEDE analysis. These data compare the instantaneous fluxes and the cumulative total amounts of ions measured in the downstream reservoirs with those fitted by MIEDE (see text for details). Data are reported for the four salinity conditions (with and without salinity gradients). Diffusive flux calculated with MIEDE for $^{22}Na^+$ for no salinity gradient conditions at 10^{-2} M NaCl was not reported due to the limitation of $^{22}Na^+$ mobility in the clay medium by that in stainless-steel filters used for experiments, leading then to propose only a lower limit for $D_e(^{22}Na^+)$ in clay medium (see Table 1 and text for details).

S.I.4 reports data measured for $^{22}Na^+$ in the specific case of the experiment performed using a fixed 10^{-2} M NaCl solution in both upstream and downstream reservoirs. These data are reported to show that constant boundary conditions with a constant $^{22}Na^+$ activity in the aqueous upstream reservoir all along the experiment could not be respected (S.I.4 a).

S.I.5 compares HDO instantaneous flux obtained experimentally with those predicted by CrunchClay considering 2 porosities ('CrunchClay 2 porosities' model). Predicted data compare calculations performed by considering activity gradient with those for which activity coefficients are neglected. Data are reported in the case of the presence of a NaCl concentration gradient between 1 M in the upstream reservoir and 0.005 M in the clay and downstream reservoir.

Acknowledgments

The results presented are part of the Ph.D. thesis of T.D. granted by "Région Nouvelle-Aquitaine", University of Poitiers, France. The authors are grateful to the CNRS interdisciplinary "défi Needs" program (Project DARIUS), the French government program "Investissements d'Avenir" (EUR INTREE, reference ANR-18-EURE-0010), the European Joint Program EURAD (WP Future – grant ID 847593) and the European Union (ERDF) and "Région Nouvelle Aquitaine" for providing financial support for this study. C.T. and C.I.S. would like to acknowledge the funding support by the Office of Science, Office of Basic Energy Sciences, Chemical Sciences, Geosciences, and Biosciences Division, through its Geoscience program at LBNL under Contract DE-AC02-05CH11231. C.T. acknowledges a grant

overseen by the French National Research Agency (ANR) as part of the “Investissements d’Avenir” Programme LabEx VOLTAIRE, 10-LABX-0100, and the EC Horizon 2020 project EURAD under Grant Agreement 847593 (WP DONUT).

References

Abend, S., Lagaly, G., 2000. Sol-gel transitions of sodium montmorillonite dispersions. Appl. Clay Sci., 2000, 16, 201−227. https://doi.org/10.1016/S0169-1317(99)00040-X

Appelo, C.A.J., Wersin, P., 2007. Multicomponent Diffusion Modeling in Clay Systems with Application to the Diffusion of Tritium, Iodide, and Sodium in Opalinus Clay. Environ. Sci. Technol. 41, 5002–5007. https ://doi.org/10.1021/es0629256

Appelo, C.A.J., Van Loon, L.R., Wersin, P., 2010. Multicomponent diffusion of a suite of tracers (HTO, Cl, Br, I, Na, Sr, Cs) in a single sample of Opalinus Clay. Geochim. Cosmochim. Acta, 74, 1201-1919. https://doi.org/10.1016/j.gca.2009.11.013

Appelo, C.A.J., 2015. Principles, caveats and improvements in databases for calculating hydrogeochemical reactions in saline waters from 0 to 200 °C and 1 to 1000 atm. Appl. Geochem, 55, 62-71. https://doi.org/10.1016/j.apgeochem.2014.11.007

Asaad, A., Hubert, F., Ferrage, E., Dabat, T., Paineau, E., Porion, P., Savoye, S., Gregoire, B., Dazas, B., Delville, A., Tertre, E., 2021. Role of interlayer porosity and particle organization in the diffusion of water in swelling clays. Appl. Clay Sci., 207, 106089. https://doi.org/10.1016/j.clay.2021.106089

Bacle, P., Dufrêche, J.-F., Rotenberg, B., Bourg, I.C., Marry, V., 2016. Modeling the transport of water and ionic tracers in a micrometric clay sample. Appl. Clay Sci., 123, 18–28. https://doi.org/10.1016/j.clay.2015.12.014

Bestel, M., Glaus, M.A., Frick, S., Gimmi, T., Juranyi, F., Van Loon, L.R., Diamond, L.W., 2018. Combined tracer through-diffusion of HTO and ^{22}Na through Na-montmorillonite with different bulk dry densities. Appl. Geochem., 93, 158–166. https://doi.org/10.1016/j.apgeochem.2018.04.008

Birgersson, M., Karnland O., 2009. Ion equilibrium between montmorillonite interlayer space and an external solution – Consequences for diffusional transport. Geochim. Cosmochim. Acta, 73, 1908-1923. https://doi.org/10.1016/j.gca.2008.11.027

Bohnhoff, G.L., Shackelford, C.D., 2014. Hydraulic Conductivity of Polymerized Bentonite-Amended Backfills. Journal of Geotechnical and Geoenvironmental Engineering, 140 (3), 04013028. https://doi.org/10.1061/(ASCE)GT.1943-5606.0001034

Bourg, I.C., Tournassat, C., 2015. Chapter 6 – Self-Diffusion of Water and Ions in Clay Barriers, in: Tournassat, C., Steefel, C.I., Bourg, I.C., Bergaya, F. (Eds.), Developments in Clay Science. Elsevier, pp. 189–226. https://doi.org/10.1016/B978-0-08-100027-4.00006-1

Bourg I.C., Bourg A.C.M., Sposito G., 2003. Modeling diffusion and adsorption in compacted bentonite: a critical review. J. Contam. Hydrol., 61, 293-302. https://doi.org/10.1016/S0169-7722(02)00128-6

Chen, Y., Glaus, M.A., Van Loon, L.R., Mader, U., 2018. Transport behaviour of low molecular weight organic compounds in multi-mineral clay systems. A comparison between measured and predicted values. Appl. Clay Sci., 165, 247-256. https://doi.org/10.1016/j.clay.2018.08.004

Charlet, L., Alt-Epping, P., Wersin, P., Gilbert, B., 2017. Diffusive transport and reaction in clay rocks: A storage (nuclear waste, CO2, H2), energy (shale gas) and water quality issue. Advances in Water Resources, 106, 39–59. https://doi.org/10.1016/j.advwatres.2017.03.019

Churakov, S.V., Gimmi, T., 2011. Up-Scaling of Molecular Diffusion Coefficients in Clays: A Two-Step Approach. J. Phys. Chem. C, 115, 6703–6714. https://doi.org/10.1021/jp112325n

Churakov, S.V., Gimmi, T., Unruh, T., Van Loon, L.R., Juranyi, F., 2014. Resolving diffusion in clay minerals at different time scales: Combination of experimental and modelling approaches. Appl. Clay Sci., 96, 36–44. https://doi.org/10.1016/j.clay.2014.04.030

Dabat, T., 2019. Anisotropie d'orientation des particules des milieux poreux argileux et implication sur la diffusion de l'eau. Université de Poitiers, Poitiers (France).

Dabat, T., Porion, P., Hubert, F., Paineau, E., Dazas B., Grégoire, B., Tertre, E., Delville, A., Ferrage, E., 2020. Influence of preferred orientation of clay particles on the diffusion of water in kaolinite porous media at constant porosity. Appl. Clay Sci., 184, 105354. https://doi.org/10.1016/j.clay.2019.105354

Descostes, M., Blin, V., Bazer-Bachi, F., Meier, P., Grenut, B., Radwan, J., Schlegel, M.L., Buschaert, S., Coelho, D., Tevissen, E., 2008. Diffusion of anionic species in Callovo Oxfordian argillites and Oxfordian limestones (Meuse/Haute-Marne, France). Appl. Geochem. 23, 655–677. https://doi.org/10.1016/j.apgeochem.2007.11.003

Didierjean, S., Maillet, D., Moyne, C., 2004. Analytical solutions of one-dimensional macrodispersion in stratified porous media by the quadrupole method: convergence to an equivalent homogeneous porous medium. Adv. Water Resour. 27, 657–667. https://doi.org/10.1016/j.advwatres.2004.02.022

Dzene, L., Ferrage, E., Hubert, F., Delville, A., Tertre, E., 2016. Experimental evidence of the contrasting reactivity of external vs. interlayer adsorption sites on swelling clay minerals: the case of Sr^{2+}-for-Ca^{2+} exchange in vermiculite. Appl. Clay Sci., 132-133, 205215. https://doi.org/10.1016/j.clay.2016.06.007

Faurel, M., 2012. Conception et mise en place d'expériences de diffusion de l'eau et de solutés dans des milieux poreux modèles d'argiles gonflantes. Université de Poitiers, France.

Ferrage, E., Hubert, F., Dabat, T., Asaad, A., Dazas, B., Gregoire, B., Savoye, S., Tertre, E. 2023. Anisotropy in particle orientation controls water diffusion in clay materials. Appl. Clay Sci., 244, 107117. https://doi.org/10.1016/j.clay.2023.107117

García-Gutierrez, M., Cormenzana, J. L., Missana, T., Mingarro, M., 2004. Diffusion coefficient and accessible porosity for HTO and ^{36}Cl, compacted FEBEX bentonite. Appl. Clay Sci., 26, 65−73. https://doi.org/10.1016/J.CLAY.2003.09.012

Gaucher, E.C., et al., 2006. Modelling the porewater chemistry of the Callovian-Oxfordian formation at a regional scale. Compte Rendus Geosciences, 338, 917-930. https://doi.org/10.1016/j.crte.2006.06.002

Gonçalvès, J., Violette, S., Wendling, J., 2004. Analytical and numerical solutions for alternative overpressuring processes: Application to the Callovo-Oxfordian sedimentary sequence in the Paris basin, France. J. Geophys. Res. Solid Earth 109. https://doi.org/10.1029/2002JB002278

Glaus, M.A., Baeyens, B., Bradbury, M.H., Jakob, A., Van Loon, L.R., Yaroshchuk, A., 2007. Diffusion of ^{22}Na and ^{85}Sr in montmorillonite: Evidence of interlayer diffusion being the dominant pathway at high compaction. Environ. Sci. Technol., 41, 478–485. https://doi.org/10.1021/es061908d

Glaus, M.A., Rossé, R., Van Loon, L.R., Yaroshchuk, A.E., 2008. Tracer diffusion in sintered stainless steel filters: measurement of effective diffusion coefficients and implications for diffusion studies with compacted clays. Clays Clay Miner., 56, 677–685. https://doi.org/10.1346/CCMN.2008.0560608

Glaus, M.A., Frick, S., Rossé, R., Van Loon, L.R., 2010. Comparative study of tracer diffusion of HTO, $^{22}Na^{+}$ and $^{36}Cl^{-}$ in compacted kaolinite, illite and montmorillonite. Geochim. Cosmochim. Acta, 74, 1999–2010. https://doi.org/10.1016/J.GCA.2010.01.010

Glaus, M. A., Birgersson, M., Karnland, O., Van Loon, L. R., 2013. Seeming steady-state uphill diffusion of $^{22}Na^{+}$ in compacted montmorillonite. Environmental Science & Technology, 47, 11522-11527. https://doi.org/10.1021/es401968c

González Sánchez, F., Van Loon, L.R., Gimmi, T., Jakob, A., Glaus, M.A., Diamond, L.W., 2008. Self-diffusion of water and its dependence on temperature and ionic strength in highly compacted montmorillonite, illite and kaolinite. Appl. Geochem., 23, 3840–3851. https://doi.org/10.1016/j.apgeochem.2008.08.008

Gueutin, P., Altmann, S., Gonçalvès, J., Cosenza, P., Violette, S., 2007. Osmotic interpretation of overpressures from monovalent based triple layer model, in the Callovo-Oxfordian at the Bure site. Phys. Chem. Earth Parts ABC, Clay in natural and engineered barriers for radioactive waste – confinement - Part 1 32, 434–440. https://doi.org/10.1016/j.pce.2005.12.002

Heister, K., Kleingeld, P.J., Gustav Loch, J.P., 2005. Quantifying the effect of membrane potential in chemical osmosis across bentonite membranes by virtual short-circuiting. J. Colloid Interface Sci., 286, 294–302. https://doi.org/10.1016/j.jcis.2005.01.044

Hedström, M., Karnland, O, 2012. Donnan equilibrium in Na-montmorillonite from a molecular dynamics perspective. Geochim. Cosmochim. Acta, 77, 266-274. https://doi.org/10.1016/j.gca.2011.11.007

Kemper, W.D., Van Schaik, J.C., 1966. Diffusion of Salts in Clay-Water Systems 1. Soil Sci. Soc. Am. J., 30, 534–540. https://doi.org/10.2136/sssaj1966.03615995003000050006x

Lake, C.B., Rowe, R.K., 2000. Diffusion of sodium and chloride through geosynthetic clay liners. Geotext. Geomembr., 18, 103–131. https://doi.org/10.1016/S0266-1144(99)00023-0

Le Crom, S., Tournassat, C., Robinet, J.C., Marry, V., 2022. Influence of Water Saturation Level on Electrical Double Layer Properties in a Clay Mineral Mesopore : A Molecular Dynamics Study. J. Phys. Chem. C, 126 (1), 647-654. https://doi.org/10.1021/acs.jpcc.1c08637

Liu, L., 2013. Prediction of swelling pressures of different types of bentonite in dilute solutions. Colloids Surf., 434, 303−318. https://doi.org/10.1016/j.colsurfa.2013.05.068

Malusis, M.A., Shackelford, C.D., 2002. Coupling Effects during Steady-State Solute Diffusion through a Semipermeable Clay Membrane. Environ. Sci. Technol., 36, 1312–1319. https://doi.org/10.1021/es011130q

Massat, L., Cuisinier, O., Bihannic, I., Claret, F., Pelletier, M., Masrouri, F., Gaboreau, S., 2016. Swelling pressure development and inter-aggregate porosity evolution upon hydration of a compacted swelling clay. Appl. Clay Sci., 124, 197-210. https://doi.org/10.1016/j.clay.2016.01.002

Mazurek, M., Alt-Epping, P., Bath, A., Gimmi, T., Niklaus Waber, H., Buschaert, S., Cannière, P. D., De Craen, M., Gautschi, A., Savoye, S., Vinsot, A., Wemaere, I., Wouters, L., 2011, Natural tracer profiles across argillaceous formations. Appl. Geochem., 26, 1035–1064. https://doi.org/10.1016/j.apgeochem.2011.03.124

Melkior, T., Gaucher, E.C., Brouard, C., Yahiaoui, S., Thoby, D., Clinard, C., Ferrage, E., Guyonnet, D., Tournassat, C., Coelho, D., 2009. Na^+ and HTO diffusion in compacted bentonite: Effect of surface chemistry and related texture. J. Hydrol., 370, 9–20. https://doi.org/10.1016/j.jhydrol.2009.02.035

Mills, R., Lobo, V.M.M., 1989. Self-diffusion in Electrolyte Solutions: A Critical Examination of Data Compiled from the Literature. Elsevier.

Moridis, G.J., 1998. A Set of Semi-analytical Solutions for Parameter Estimation in Diffusion cell Experiments. Report LBNL-41857. Lawrence Berkeley National Laboratory, Berkeley, California.

Muurinen, A., Olin, M., Uusheimo, K., 1989. Diffusion of Sodium and Copper in Compacted Sodium Bentonite at Room Temperature. MRS Online Proc. Libr. Arch. 176. https://doi.org/10.1557/PROC-176-641

Pearson, F. J., Tournassat, C., Gaucher, E. C., 2011, Biogeochemical processes in a clay formation in situ experiment: Part E - Equilibrium controls on chemistry of pore water from the Opalinus Clay, Mont Terri Underground Research Laboratory, Switzerland. Appl. Geochem., 26, 990–1008. https://doi.org/ 10.1016/j.apgeochem.2011.03.008

Radwan, J., Hainos, D., Grenut, B., 2006. Qualification expérimentale de la plate-forme ALLIANCES. 1ère partie: Calculs préliminaires. Technical report, CEA, Gif sur Yvette, France.

Reinholdt, M.X., Hubert, F., Faurel, M., Tertre, E., Razafitianamaharavo, A., Francius, G., Prêt, D., Petit, S., Béré, E., Pelletier, M., Ferrage, E., 2013. Morphological properties of vermiculite particles in size-selected fractions obtained by sonication. Appl. Clay Sci., 77–78, 18–32. https://doi.org/10.1016/j.clay.2013.03.013

Rotenberg, B., Marry, V., Salanne, M., Jardat, M., Turq, P., 2014. Multiscale modelling of transport in clays from the molecular to the sample scale. Comptes Rendus Geosci., 346, 298–306. https://doi.org/10.1016/J.CRTE.2014.07.002

Savoye, S., Frasca, B., Grenut, B., Fayette, A., 2012. How mobile is iodide in the Callovo–Oxfordian claystones under experimental conditions close to the in situ ones? J. Contam. Hydrol., 142, 82–92. https://doi.org/10.1016/j.jconhyd.2012.10.003

Soler, J. M., Steefel, C. I., Gimmi, T., Leupin, O. X., Cloet, V., 2019. Modeling the ionic strength effect on diffusion in clay. The DR-A experiment at Mont Terri. ACS Earth and Space Chemistry, 3, 442-451. https://doi.org/10.1021/ACSEARTHSPACECHEM.8B00192

Steefel, C. I., Tournassat, C., 2021. A model for discrete fracture-clay rock interaction incorporating electrostatic effects on transport. Computational Geosciences, 25, 395-410. https://doi.org/10.1007/s10596-020-10012-3

Tertre, E., Savoye, S., Hubert, F., Prêt, D., Dabat, T., Ferrage, E., 2018. Diffusion of water through the dual porosity swelling clay mineral vermiculite. Environ. Sci. Technol., 52, 1899 -1907. https://doi.org/10.1021/acs.est.7b05343

Tournassat, C., Appelo, C. A. J., 2011. Modelling approaches for anion-exclusion in compacted Na-bentonite. Geochim. Cosmochim. Acta, 75, 3698-3710. https://doi.org/10.1016/j.gca.2011.04.001

Tournassat, C., Steefel, C.I., 2015. Ionic Transport in Nano-Porous Clays with Consideration of Electrostatic Effects. Rev. Mineral. Geochem., 80, 287–329. https://doi.org/10.2138/rmg.2015.80.09

Tournassat, C., Bourg, I.C., Holmboe, M., Sposito, G., Steefel, C.I., 2016. Molecular dynamics simulations of anion exclusion in clay interlayer nanopores. Clays Clay Miner., 64, 374–388. https://doi.org/10.1346/CCMN.2016.0640403

Tournassat, C., Steefel, C. I., 2019. Reactive transport modelling of coupled processes in nanoporous media. Reviews in Mineralogy and Geochemistry, 85, 75-110. https://doi.org/10.2138/rmg.2019.85.4

Tournassat, C., Steefel, C. I., 2020. Modeling diffusion processes in the presence of a diffuse layer at charged mineral surfaces. A benchmark exercise. Computational Geosciences, 25 (4), 1319-1336. https://doi.org/10.1007/s10596-019-09845-4

Tyagi, M., Gimmi, T., Churakov, S.V., 2013. Multi-scale micro-structure generation strategy for up-scaling transport in clays. Adv. Water Resour., 59, 181–195. https://doi.org/10.1016/j.advwatres.2013.06.002

Van Brakel, J., Heerthes, PM, 1974. Analysis of diffusion in microporous media in terms of a porosity, a tortuosity and a constrictivity factor. Intern. J. Heat and Mass Transfer, 17 (9), 1093-1103. https://doi.org/10.1016/0017-9310 (74)90190-2

Van Loon, L.R., Glaus, M.A., Müller, W., 2007. Anion exclusion effects in compacted bentonites: Towards a better understanding of anion diffusion. Applied Geochem., 22, 2536–2552. https://doi.org/10.1016/j.apgeochem.2007.07.008

Van Schaik, J.C., Kemper, W.D., 1966. Chloride Diffusion in Clay-Water Systems. Soil Sci. Soc. Am. J., 30, 22–25. https://doi.org/10.2136/sssaj1966.03615995003000010014x

Wang, J., Savoye, S., Ferrage, E., Hubert, F., Lefevre, S., Radwan, J., Robinet, J. C., Tertre, E., Gouze, P., 2022. Water and ion diffusion in partially-water saturated compacted kaolinite: role played by vapor-phase diffusion in water mobility. J. Contam. Hydrol., 248, 103989. https://doi.org/10.1016/j.jconhyd.2022.103989

Wersin, P., Mazurek, M., Mäder, U. K., Gimmi, T., Rufer, D., Lerouge, C., Traber, D., 2016. Constraining porewater chemistry in a 250 m thick argillaceous rock sequence: Chem. Geol., 434, 43–61. https://doi.org/10.1016/j.chemgeo.2016.04.006

Wigger, C., Van Loon, L.R., 2017. Importance of interlayer equivalent pores for anion diffusion in clay-rich sedimentary rocks. Environ. Sci. Technol., 51, 1998 -2006. https://doi.org/10.1021/acs.est.6b03781

Table caption

Table 1: Summary of diffusion experiments, including characteristics of the compacted samples, and diffusion parameters (effective diffusion coefficient and rock capacity factor) used to interpret experimental data with MIEDE. Inverse of geometrical factor (i.e., $\frac{1}{G}$) values obtained with MIEDE and used with CrunchClay® to interpret experimental data are also reported (see text for details).

Figure caption

Fig. 1: Description of multi-scale organization of vermiculite dual-porosity media (adapted from Ferrage et al., 2023). (a) Scale of the crystal structure of vermiculite with interlayer pore space. (b) Scale of the individual vermiculite particle with interparticle (①) and interlayer porous network (②). (c) Scale of a stack of particles of ~1 μm^3 dimension.

Fig. 2: Comparison between effective diffusion coefficients (D_e) measured in this study for porous media made of vermiculite with those reported from literature and obtained for media made with other types of clays. Data are plotted as a function of the salinity of the upstream reservoir and data from literature are obtained for porous media having either total porosity or interparticle porosity close to that of the vermiculite sample used in this study. Data obtained with salinity gradients are plotted as open symbols while those obtained without salinity gradients are represented as closed symbols. Cl^-: left panel; Na^+: right panel.

Fig. 3: Comparison between instantaneous flux measured in the downstream reservoirs (symbols) with those predicted using CrunchClay® software (lines; see details of the model in text). Data are reported for no salinity gradient conditions for the three tracers: HTO, $^{36}Cl^-$ and $^{22}Na^+$.

A: 1 M for both upstream and downstream reservoirs. B: 10^{-2} M for both upstream and downstream reservoirs. Data fitted with MIEDE are also reported for information (see details in the text and in S.I.3 and 4), except for $^{22}Na^+$ for 10^{-2}M constant salinity conditions because of the limitation of $^{22}Na^+$ mobility in the clay medium by that in stainless-steel filters (see text for details).

Fig. 4: Comparison between instantaneous flux measured in the downstream reservoirs (symbols) with those predicted using CrunchClay® software (lines; see details of the model in text). Data are reported for salinity gradient conditions for the three tracers: HDO, Cl^- and Na^+.

A: 1 M for the upstream reservoir, pure water for downstream reservoir; B: 10^{-2} M for the upstream reservoir, pure water for downstream reservoir. Data fitted with MIEDE are also reported for information (see details in the text and in S.I.3 and 4).

total porosity ε^a ± 0.025	**interparticle porosity $\varepsilon_{interp}{}^b$ ± 0.025**	**thickness of compacted sample L (mm) ± 0.1**	**presence of salinity gradient**	**chemical composition of the upstream reservoir (M or Bq L^{-1})**	**chemical composition of the downstream reservoir (M)**	**D_e (20°C) ($\times 10^{-10}$ m^2 s^{-1}) obtained by MIEDE**	**α obtained by MIEDE**	**$\frac{1}{G}$ (20°C) obtained by MIEDE for HTO/HDO (*i.e.*, D_p/D_0) and used in CrunchClay predictions**
0.490	0.250	8.0	No	- [HTO]=8.03 10^{-10} M (i.e., 8.6 10^5 Bq/L) - [Cl^-]=10^{-2} M - [Na^+]=10^{-2} M - [$^{36}Cl^-$]=1.07 10^{-5} (i.e., 4.7 10^5 Bq/L) - [$^{22}Na^+$]=1.32 10^{-10} (i.e., 6.7 10^5 Bq/L)	- [HTO]=0 - [Cl^-]=10^{-2} - [Na^+]=10^{-2} - [$^{36}Cl^-$]=0 - [$^{22}Na^+$]=0	HTO : 2.0 (1.5-2.8) $^{36}Cl^-$: 0.14 (0.11-0.17) $^{22}Na^+$: > 20[c]	HTO : 0.49 (0.45-0.54) $^{36}Cl^-$: 0.30 (0.25-0.35) $^{22}Na^+$: >750[c]	0.19
0.490	0.250	8.0	No	- [HTO]=1.2 10^{-9} M (i.e., 1.29 10^6 Bq/L) - [Cl^-]=1 M - [Na^+]=1 M - [$^{36}Cl^-$]=1.13 10^{-5} M (i.e., 5 10^5 Bq/L) - [$^{22}Na^+$]=1.23 10^{-10} M (i.e., 6.3 10^5 Bq/L)	- [HTO]=0 - [Cl^-]=1 - [Na^+]=1 - [$^{36}Cl^-$]=0 - [$^{22}Na^+$]=0	HTO : 2.4 (1.8-3.2) $^{36}Cl^-$: 1.5 (1.1-2.0) $^{22}Na^+$: 2.3 (1.8-2.9)	HTO : 0.49 (0.45-0.50) $^{36}Cl^-$: 0.3 (0.3-0.4) $^{22}Na^+$: 3.2 (3.0-3.4)	0.23
0.495	0.250	8.0	Yes	- [HDO]=0.56 M - [Cl^-]=0.01 M - [Na^+]=0.01 M	- [HDO]=1.65 10^{-2} - [Cl^-] < 10^{-5} - [Na^+] <10^{-5}	HDO : 1.8 (1.4-2.2) Cl^- : 0.18 (0.12-0.23) Na^+ : 0.35	HDO : 0.49 (0.49-0.7) Cl^- : 0.1 (0.05-0.40) Na^+ : 0.49	0.17

						(0.28-0.42)	(0.1-0.49)	
0.495	0.250	8.0	Yes	- [HDO]=0.57 M - [Cl^-]=0.99 M - [Na^+]=0.99 M	- [HDO]=1.65 10^{-2} - [Cl^-] < 10^{-5} - [Na^+] <10^{-5}	HDO : 1.8 (1.6-2.1) Cl^- : 1.8 (1.5-2.0) Na^+ : 2.1 (1.8-2.6)	HDO : 0.49 (0.49-0.8) Cl^- : 0.49 (0.49-1) Na^+ : 0.49 (0.49-1)	0.17

Table 1

[a] calculated as $\varepsilon = 1-\rho_{app.}/\rho_s$ where ρ_s is the real grain density (i.e., 2.7 g cm^{-3} as calculated by Reinholdt et al. (2013) on the basis of the structural formula). $\rho_{app.}$ is the bulk dry density (i.e., 1.49 g cm^{-3}) calculated considering the volume of diffusion cell and the mass of samples measured at 25 °C and corrected from mass of interlayer water of Na-vermiculite at room humidity (approximatively 10 %) as performed in previous studies (Tertre et al., 2018; Asaad et al., 2021).

[b] ε_{interp} is calculated as detailed in Asaad et al. (2021).

[c] Constant boundary conditions were not reached for this experiment, and $^{22}Na^{+}$ mobility in the clay medium was limited by that in the stainless-steel filters; then only lower limit of the diffusion parameter values could be estimated for $^{22}Na^{+}$ using MIEDE (see text for details).

Table 1: Summary of diffusion experiments, including characteristics of the compacted samples, and diffusion parameters (effective diffusion coefficient and rock capacity factor) used to interpret experimental data with MIEDE. Inverse of geometrical factor (i.e., $\frac{1}{G}$) values obtained with MIEDE and used with CrunchClay® to interpret experimental data are also reported (see text for details).

Credit Author Statement

Emmanuel Tertre: Investigation, Conceptualization, Formal analysis, Writing - Original Draft,
Visualization, Writing - Review & Editing, Project administration.
Thomas Dabat: Investigation, Formal analysis, Visualization, Review & Editing.
Jingyi Wang: Investigation, Formal analysis, Review & Editing.
Sébastien Savoye: Investigation, Formal analysis, Visualization, Review & Editing.
Fabien Hubert: Investigation, Review & Editing.
Baptiste Dazas: Investigation, Review & Editing.
Christophe Touranssat: Investigation, Conceptualization, Visualization, Formal analysis, Review & Editing.
Carl I. Steefel: Visualization, Review & Editing.
Eric Ferrage: Conceptualization, Visualization, Review & Editing, Project administration.

All authors have read and agreed to the published version of the manuscript.

Declaration of interests

☒The authors declare that they have no known competing financial interests or personal relationships that could have appeared to influence the work reported in this paper.

☐The authors declare the following financial interests/personal relationships which may be considered as potential competing interests:

Highlights

- Effect of salinity gradients on the diffusion properties of ions in porous clayey media
- Role played by interparticle and interlayer porosities on diffusion properties
- Reactive transport modeling to interpret through-diffusion experimental data

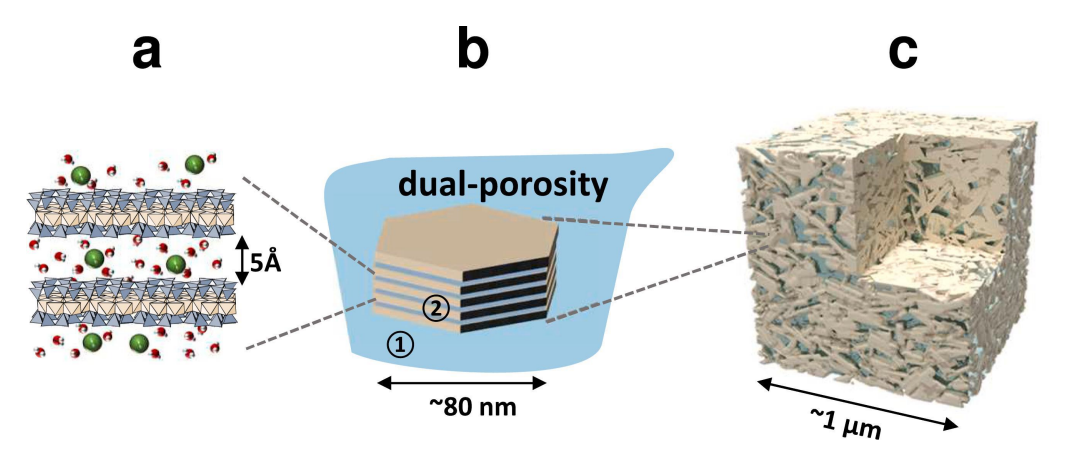

Figure 1

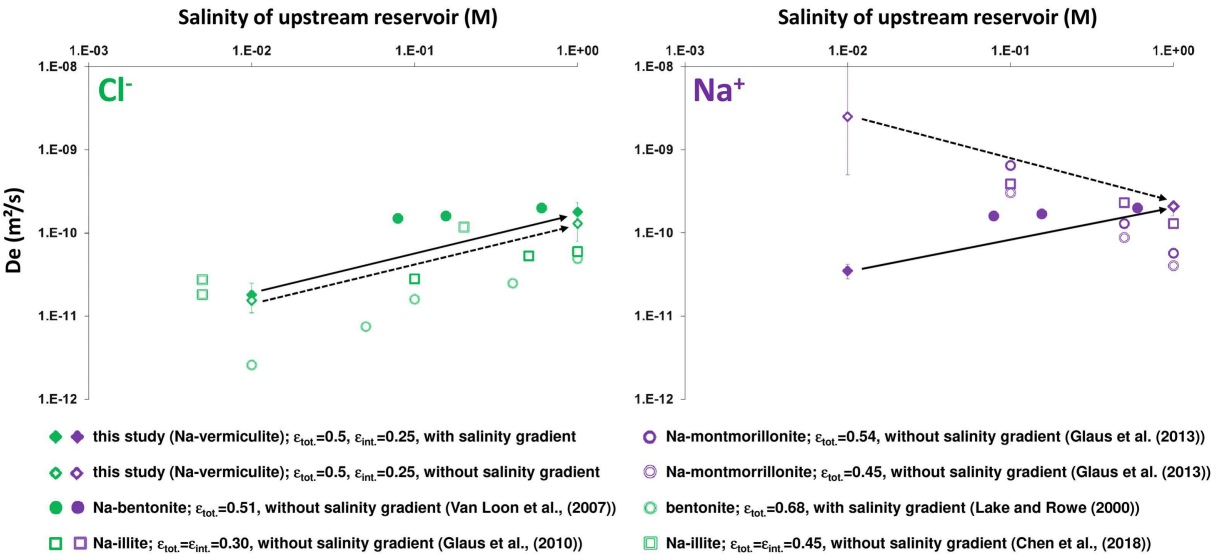
Salinity of upstream reservoir (M)
1.E-03
1.E-02
1.E-01
1.E+00
1.E-08
1.E-09
1.E-10
1.E-11
1.E-12
De (m²/s)
Cl⁻
Na⁺
this study (Na-vermiculite); ε_tot.=0.5, ε_int.=0.25, with salinity gradient
this study (Na-vermiculite); ε_tot.=0.5, ε_int.=0.25, without salinity gradient
Na-bentonite; ε_tot.=0.51, without salinity gradient (Van Loon et al., (2007))
Na-illite; ε_tot.=ε_int.=0.30, without salinity gradient (Glaus et al., (2010))
Na-montmorillonite; ε_tot.=0.54, without salinity gradient (Glaus et al. (2013))
Na-montmorrillonite; ε_tot.=0.45, without salinity gradient (Glaus et al. (2013))
bentonite; ε_tot.=0.68, with salinity gradient (Lake and Rowe (2000))
Na-illite; ε_tot.=ε_int.=0.45, without salinity gradient (Chen et al., (2018))

Figure 2

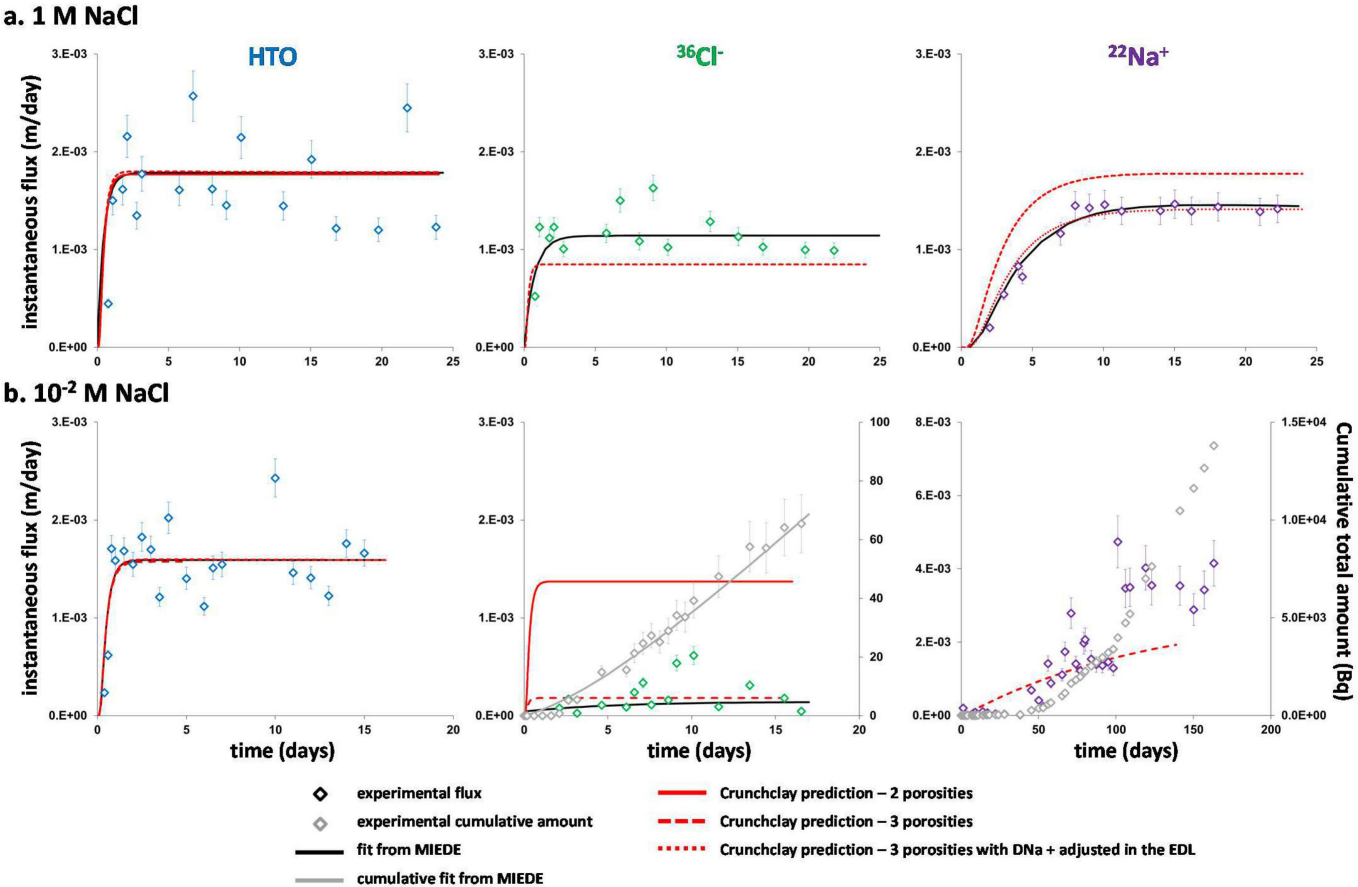
a. 1 M NaCl
HTO
36Cl-
22Na+
b. 10-2 M NaCl
instantaneous flux (m/day)
time (days)
Cumulative total amount (Bq)
experimental flux
experimental cumulative amount
fit from MIEDE
cumulative fit from MIEDE
Crunchclay prediction – 2 porosities
Crunchclay prediction – 3 porosities
Crunchclay prediction – 3 porosities with DNa + adjusted in the EDL

Figure 3

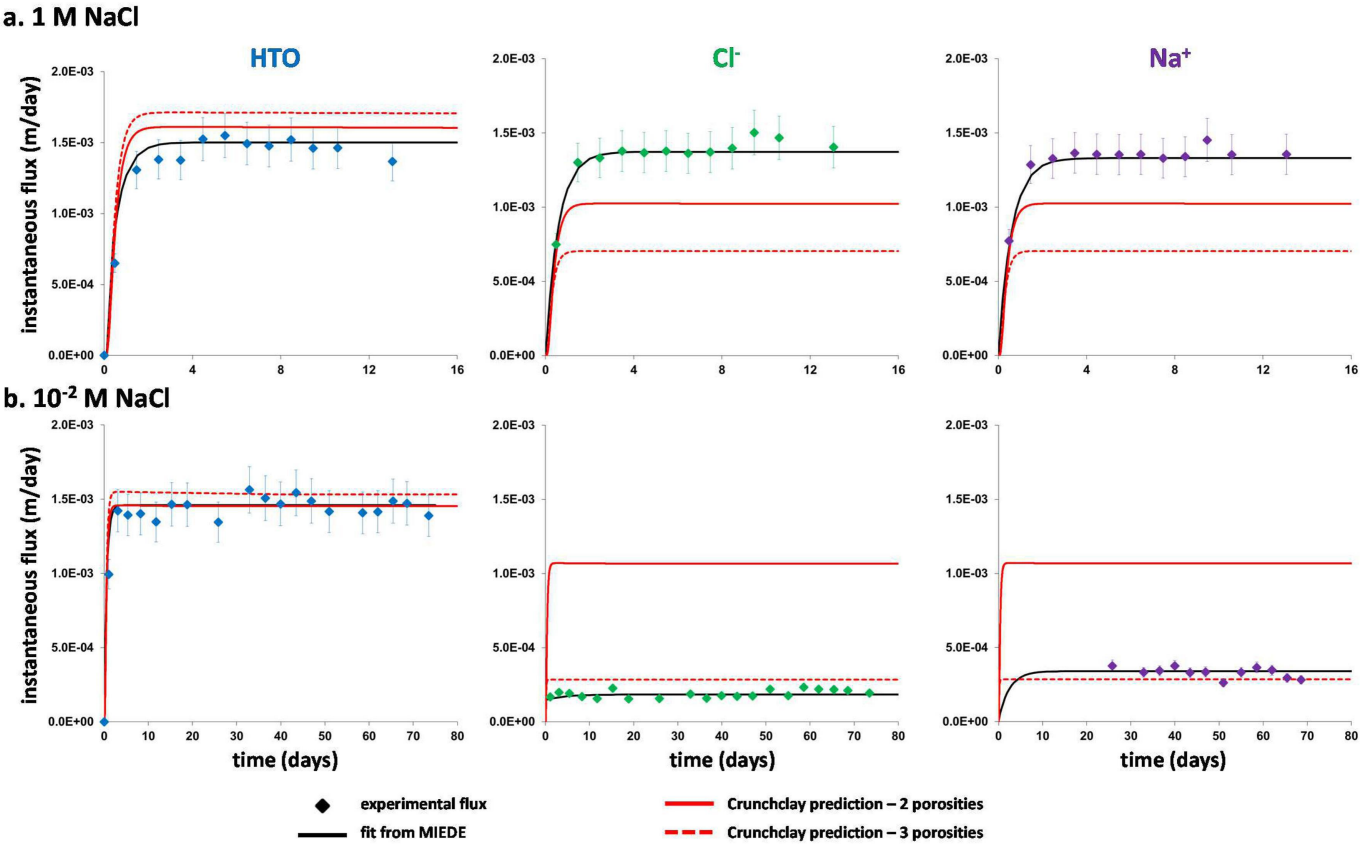
a. 1 M NaCl
HTO
Cl-
Na+
b. 10-2 M NaCl
instantaneous flux (m/day)
time (days)
experimental flux
fit from MIEDE
Crunchclay prediction – 2 porosities
Crunchclay prediction – 3 porosities

Figure 4